

The structure and dynamics of dipolar vortices in a stratified fluid

By OLIVIER PRAUD AND ADAM M. FINCHAM†

Laboratoire des Ecoulements Géophysiques et Industriels (LEGI) CNRS-UJF-INPG, Coriolis,
BP53, 38041 Grenoble, cedex9, France

(Received 28 August 2002 and in revised form 4 April 2005)

The three-dimensional structure and decay of a dipolar vortex in a linearly stratified fluid is investigated experimentally using a high-resolution three-dimensional scanning correlation image velocimetry system (SCIV). Comparisons with simple theoretical and numerical models are made for late times in the low-Froude-number regime. The relatively well-known stratified dipole, most of the time assumed to be quasi-two-dimensional, is revealed to have a complex three-dimensional vortex topology arising from its self-induced propagation. As the buoyancy scale u/N approaches zero the dynamics of such a structure are dominated by the horizontal velocity field, whereas the diffusion is mainly vertical. The evolution is then governed by an effective Reynolds number, Re_{eff} , based on vertical diffusion and horizontal advection. At early times this effective Reynolds number is large, horizontal advection terms dominate and a decrease of aspect ratio of the structure is observed until Re_{eff} reaches a critical value $Re_{eff}^c \sim O(1)$, independent of the initial condition and associated with a horizontal advection–vertical diffusion balance. Thereafter the evolution becomes purely diffusive with decay time Re_{eff}^c .

1. Introduction

One hypothesis for the approach to the final state of decaying stratified turbulence characterizes it as a field of quasi-two-dimensional vortices. A common feature observed among these vortices is the dipolar vortex, which consists of two closely spaced patches of oppositely signed vorticity. Such vortices are frequently observed in both the ocean and atmosphere (Fedorov & Ginsburg 1989), where they are believed to play an important role in transport and mixing, over a wide range of scales. This relevance to geophysical flow systems is largely responsible for the extensive studies of dipolar vortex dynamics performed over the last few decades. Though associated with a characteristic two-dimensional signature, these dipoles, like all real vortices, are inherently three-dimensional.

The two-dimensional counterparts of such structures have been investigated in various numerical and theoretical studies (Swaters 1988; Nielsen & Rasmussen 1997; van Geffen & van Heijst 1998). In the laboratory, the emergence of quasi-two-dimensional dipolar structures, their stability and their dynamical properties have been studied in several different types of experiments: Couder & Basdevant (1986) generated dipoles in a thin soap film, while Nguyen Duc & Sommeria (1988)

† Present address: University of Southern California, AME Dept, Los Angeles, CA 90089-1191, USA.

used magnetohydrodynamics to two-dimensionalize the flow. Experimental studies have also been performed in plasmas (Huld *et al.* 1991) and strong rotation has also been used to confine the dimensionality of the flow (Hopfinger, Browand & Gagne 1982). Sous, Bonneton & Sommeria (2004) have recently generated quasi-two-dimensional dipoles through confinement in shallow water layers. Experiments in stratified fluids show similarity to two-dimensional vortex dynamics (Voropayev, Afanasyev & Filippov 1991; Flór & van Heijst 1994) but the flows behave in a much more dissipative way. Stratification alone does not two-dimensionalize the flow; it inhibits vertical displacements, producing – to first order – horizontal flow. Nevertheless, the coherent structures emerging in such flows are usually described well by two-dimensional models and in many of the earlier studies the dipolar vortex was considered and described as a purely two-dimensional structure.

In stratified fluids these low-aspect-ratio vortices can emerge from an initially turbulent flow (Lin & Pao 1979) but the tendency for initially columnar vortices to decorrelate vertically, forming layers (Fincham 1994; Billant, Chomaz & Huerre 2000; Billant & Chomaz 2000), demonstrates the inherently three-dimensional nature of strongly stratified flows. Work by Fincham, Maxworthy & Spedding (1996); Spedding, Browand & Fincham (1996); Bonnier (1999); Bonnier, Eiff & Bonneton (2000); Beckers *et al.* (2001); Beckers, Clercx & van Heijst (2002) has shed much light on the three-dimensional structure and dynamics of these pancake-like vortices. The vertical growth of these vortices has been studied in sphere wakes (Chomaz *et al.* 1993; Spedding 2002) dipoles (Flór, van Heijst & Delfos 1995) and box filling turbulence (Fincham *et al.* 1996; Praud, Fincham & Sommeria 2005). Voropayev *et al.* (1991), Bonnier *et al.* (2000) and Beckers *et al.* (2002) all measured density profiles through these vortices, while the latter authors developed a three-dimensional model. Gourlay *et al.* (2001) performed direct numerical simulations of stratified wake flows, allowing detailed examination of the vortex topology.

The present study (an initial version of which is presented in Praud & Fincham 2000) deals with the viscous decay of a three-dimensional dipolar vortex in a stably stratified fluid. Unlike previous studies, the combined effects of vertical diffusion and horizontal advection are considered. The dipole is generated by a short horizontal injection of fluid, i.e. by introduction of a horizontal impulse. The focus is on the three-dimensional structure and evolution of the dipolar vortex. The novel measurement technique used permits volumetric resolution of the three components of vorticity in time and allows the direct assimilation of the experimental data into a simple three-dimensional numerical model, which is shown to accurately describe the late time evolution of the coherent structure. A profound difference with the purely two-dimensional description will be shown; this arises from the vertical variability of the dipole's self-propagation velocity, which tends to deform the vortical structure, decorrelating the different levels. In contrast to the planar models, the kinetic energy is mainly dissipated by these strong vertical gradients. A balance argument between horizontal advection is used to define two evolutionary regimes. At early times the advection dominates and a decrease of the aspect ratio is observed while for late times the evolution is purely diffusive.

The experimental arrangement is described in §2 which is followed in §3 by the presentation of the scaling analysis used to build the model. Section 4 presents experimental observations and a description of the structure which is compared with numerical results from the model in §5, where a model for a three-dimensional Lamb–Chaplygin dipole is introduced as an initial condition for higher Reynolds number simulations. Finally, results concerning the advective–diffusive balance are presented in §6.

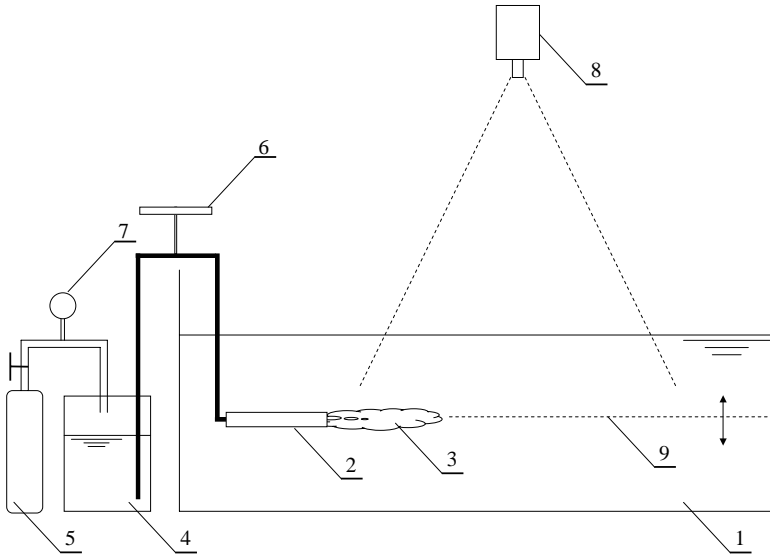


FIGURE 1. Sketch of experimental set-up: 1, tank filled with a linearly stratified salt solution; 2, horizontal injection nozzle; 3, injected turbulent region; 4, pressurized water supply system; 5, compressed air bottle; 6, computer controlled butterfly valve; 7, manometer; 8, 768×484 pixel digital camera; 9, horizontal, scanning laser sheet.

2. Experimental set-up and procedure

2.1. Experimental set-up

The experiments were performed in the 13 m diameter, 110 cm deep Coriolis platform in Grenoble, France. The tank was linearly stratified with common salt by diluting an ultrasonically maintained constant-head filling flow with a prescribed flux of brine provided by a computer controlled volumetric pump. The Brunt–Väisälä frequency of the stable stratification was 0.3 rad s^{-1} and was kept constant for all the experiments discussed here. To generate the dipolar vortices the turbulent injection method of Flór & van Heijst (1994) and Voropayev, Afanasyev & van Heijst (1995) was employed. An isolated turbulent region was created (at $t = 0 \text{ s}$) by a horizontal pulsed injection of a small volume of fluid ($0.2 < V < 1.5 \text{ l}$) through a relatively thin nozzle of diameter $d = 1.7 \text{ cm}$, during a short period of time ($1 < t < 8 \text{ s}$). This turbulent patch subsequently collapses under gravity, forming a thin pancake-like region of horizontal motion that reorganizes into a dipolar structure. The injection nozzle (that was bevelled on the outside to a fine edge) was positioned at the half-depth and particular care was taken to ensure that the density of the injected fluid exactly matched the density of the ambient fluid at the level of the injection. The slightly pressurized injection process was controlled by a stepper motor, that opened and closed a simple butterfly valve, allowing precise control of the injection parameters (i.e. volume and time of injection). The Reynolds number based on the injection parameters $Re_i = U_i d / \nu$ (U_i the jet exit velocity and ν the kinematic viscosity) was larger than 10 000 ensuring a fully turbulent jet flow at the exit of the tube. A high-resolution scanning digital particle imaging velocimetry system was used to provide components and their spacial derivatives along x , y and z of the horizontal velocity in a volume. Stepper motors drove a profiling conductivity probe used to measure density profiles. Figure 1 shows a diagram of the experimental set-up.

2.2. PIV measurement in a volume

In these experiments, the correlation imaging velocimetry (CIV) technique of Fincham & Spedding(1997) was used to determine quantitatively the velocity field in a relatively large number of horizontal planes. This multi-planar technique is referred to as scanning correlation imaging velocimetry (SCIV) (Fincham 1998). The fluid was seeded with 600 micron diameter polystyrene beads, that were carefully prepared by a process of cooking and successive density separations to have a flat distribution of densities matching that of the background stratification. This process ensured that there were equal number densities of particles at each depth. A photographic surfactant (Ilfotol) was added to the working fluid in small concentrations to prevent the polystyrene beads from agglomerating. Coherent light originating from an 8 W argon laser was directed into an optical fibre, the other end of which was attached to an optical assembly that directed the light onto a small oscillating mirror, creating a vertical light sheet. The entire optical assembly was fixed to a high-speed, horizontally displacing, computer controlled linear bearing traverse. The horizontally moving vertical light sheet passes through a thin glass plate, held parallel to and just touching the surface of the water, above a submerged 45° mirror. In this way, horizontal motion of the vertical light sheet above the water translated directly into vertical motion of a horizontal light sheet within the fluid. Due to the refractive index variation with depth, an initially horizontal beam of light will tend to curve downwards parabolically. In order to minimize this effect, only relatively weak stratifications were used and the angle of the horizontal light sheet was inclined upwards a few degrees, until the summit of its parabolic trajectory corresponded to the centre of the measurement area. This approach produced maximum deviations from horizontality that occurred at the edges of the images and were limited to about 5 mm, values close to the actual light-sheet thickness.

The volume scanning process proceeded as follows, an initial scan through all depths was made with continuous image acquisition to memory; the light sheet was then quickly returned to the starting position; after an appropriate time interval, the scan process was repeated to acquire the second image in each pair. The images were acquired by a 768×484 pixels 8-bit Pulnix 9701 interline transfer CCD camera operating at 30 frames per second in digital output mode, the camera being placed 4 m above the water surface. Each slice (corresponding to a pair of image) is treated as described in Fincham & Spedding (1997) and Fincham & Delerce (2000). Typical measurement conditions produce $80 \times 60 \times 50$ independent vectors in a volume of $250 \times 250 \times 50 \text{ cm}^3$. A combination of numerical simulations of the scanning technique and actual hardware tests using real particles ‘frozen’ inside a clear resin block, along with tests on stagnant fluid, showed that under optimum conditions, the measured mean r.m.s. error in velocity is less than 2%.

3. Theoretical and numerical models

3.1. Scaling analysis and governing equations

The low-Froude-number theory was first developed by Riley, Metcalfe & Weissman (1981) and Lilly (1983). Riley *et al.* (1981) showed that for a buoyancy-dominated, initially isotropic turbulent flow, flow fields – to lowest order – can be decomposed into vertical motions induced by internal gravity waves and quasi-horizontal turbulent motions (stratified turbulence). We will follow their scaling analysis closely.

The equations of motion for an incompressible fluid are first written in the Boussinesq approximation. Molecular diffusion of salt is very slow and its effect

is assumed to be negligible (the Schmidt number for salt water is very large compare to unity: $Sc \sim 700$)

The horizontal velocity is scaled with a characteristic horizontal velocity scale U . The horizontal and vertical directions are scaled respectively with a horizontal and vertical length scale L_h and σ . The time is scaled with the advective time scale L_h/U . Horizontal pressure gradients are assumed to be of the same order as the horizontal accelerations implying that the scale for the pressure is $\bar{\rho}U^2$ where $\bar{\rho}$ is a constant reference density. Since the vertical motions are small, the vertical momentum equation describes to good approximation a hydrostatic balance and the density perturbation is scaled as $\rho \sim \bar{\rho}U^2/(g\sigma)$ with $\mathbf{g} = (0, 0, -g)$ the gravity vector. The vertical velocity u_z is scaled as $U^3/(\sigma L_h N^2)$.

The relative importance of inertial forces in comparison to buoyancy forces is measured by the horizontal Froude number $Fr_h = U/L_h N$, which is the ratio of inertial to buoyancy time scales where, $N = \sqrt{-(g/\bar{\rho})\partial\rho_0/\partial z}$ is the Brunt–Väisälä frequency and $\rho_0(z)$ the linear mean density profile. The vertical Froude number, $Fr_v = U/\sigma N$, compares the vertical scale, σ , to the buoyancy scale, $L_b = U/N$ and is related to the horizontal Froude number through the relation $Fr_h = \alpha Fr_v$ where $\alpha = \sigma/L_h$ is the aspect ratio.

In the limit $Fr_v \rightarrow 0$, and keeping the same notation for the dimensionless variables the lowest-order equations become

$$\frac{\partial \mathbf{u}_h}{\partial t} + \mathbf{u}_h \cdot \nabla_h \mathbf{u}_h = -\nabla_h p + \frac{1}{Re} \left(\nabla_h^2 \mathbf{u}_h + \frac{1}{\alpha^2} \frac{\partial^2 \mathbf{u}_h}{\partial z^2} \right), \quad (3.1)$$

$$\nabla_h \cdot \mathbf{u}_h = 0, \quad (3.2)$$

$$0 = -\frac{\partial p}{\partial z} - \rho, \quad (3.3)$$

$$\frac{\partial \rho}{\partial t} + \mathbf{u}_h \cdot \nabla_h \rho - u_z = 0, \quad (3.4)$$

where \mathbf{u}_h is the horizontal velocity, u_z the vertical velocity and ∇_h the gradient operator working in the horizontal directions. The detailed low-Froude-number scaling argument can be found as originally derived in Riley *et al.* (1981) and reviewed in Riley & Lelong (2000). A more formal derivation can be found in Embid & Majda (1998).

This scaling analysis requires Fr_v to be small; this can be tested in our experiments. Just after the collapse of the three dimensional turbulent patch, during the dipole formation, the vertical Froude number has a value of $O(1)$. However, as the dipole decays, Fr_v rapidly decreases to values smaller than the initial value satisfying $Fr_v \ll 1$. Previous experimental studies (Flór & van Heijst 1994; Flór *et al.* 1995; Bonnier *et al.* 2000; Billant *et al.* 2000; Fincham *et al.* 1996; Godefert & Staquet 2003; Praud *et al.* 2005), also show that the vertical Froude number is initially order one but rapidly decreases to reach much smaller values.

The lowest order equation for the vertical vorticity ω_z ,

$$\frac{\partial \omega_z}{\partial t} + \mathbf{u}_h \cdot \nabla_h \omega_z = \frac{1}{Re} \left(\nabla_h^2 \omega_z + \frac{1}{\alpha^2} \frac{\partial^2 \omega_z}{\partial z^2} \right), \quad (3.5)$$

obtained by taking the curl of (3.1), demonstrates that the vertical vorticity satisfies the two-dimensional Navier–Stokes equations and is completely decoupled from the vertical motion. Nevertheless, ω_z and the horizontal velocity field may have vertical

structure. Moreover, the lowest order vertical vorticity equation has no Froude number dependence.

The pressure field is obtained by taking the horizontal divergence of (3.1), as a solution of the following cyclostrophic balance equation:

$$\nabla_h^2 p = -\nabla_h \cdot (\mathbf{u}_h \cdot \nabla_h \mathbf{u}_h). \quad (3.6)$$

The density perturbation, ρ , is then obtained from (3.3). The vertical velocity, u_z , is finally determined from (3.4), which implies that the fluid particles follow the isopycnal surfaces.

3.2. Numerical investigation

In order to investigate the temporal evolution of the dipolar vortex we numerically integrate (3.5). The nonlinear (advective) term is calculated explicitly by using the two-dimensional composite corrected Lax–Friedrichs scheme described in Liska & Wendroff (1998). The viscous term is treated implicitly using the usual Crank–Nicolson technique. The time-advancement of the numerical scheme is thus second-order accurate in time.

Given the vertical vorticity field, $\omega_z^n(x, y, z)$ at time step n , the streamfunction is computed, in physical space, at each level z , from the Poisson equation $\nabla_h^2 \psi^n = -\omega_z^n$. In order to avoid spurious effects resulting from the boundary conditions, the domain of integration is enlarged four times by setting $\omega_z = 0$ in the outer potential region. The horizontal velocity field, $\mathbf{u}_h^n(x, y, z)$, is obtained by calculating the horizontal derivatives of ψ^n at each level. This ensures that the incompressibility condition for the leading order of the horizontal velocity field (3.2) is respected. The vertical vorticity field, advected by the horizontal velocity field (v_x^n, v_y^n) , is then computed for the new time-step $n + 1$. The boundary conditions are such that ω_z must vanish at the boundaries.

Two different types of numerical simulations were done: one initialized with a three-dimensional model of the dipolar structure and the other initialized with the experimentally measured vertical vorticity field obtained directly from the volumetric SCIV data. All the numerical simulations were run in a domain of horizontal dimension $8L_h$ and vertical dimension $2L_h$. In the simulations initialized with the dipole model, the horizontal direction is discretized with 201 gridpoints and the vertical direction with 101 gridpoints, while in the simulations initialized with laboratory data the horizontal and vertical directions are both discretized with 128 gridpoints.

The density field is obtained by differentiating in z the pressure field obtained from the physical space solution of the Poisson equation (3.6), in a domain of integration enlarged four times by setting $\mathbf{u}_h = 0$ in the outer potential region.

4. Laboratory observations

4.1. Self-induced deformation

After the pulsed injection, an isolated turbulent region forms, which quickly collapses under gravity to form a thin quasi-horizontal pancake-like turbulent patch. This patch subsequently reorganizes to form a dipolar structure. During the collapse of the three-dimensional turbulent region, internal waves are generated, which radiate away from the structure and are quickly dissipated, in particular, after being reflected at the walls of the large tank. These waves are believed to play no significant role in the further evolution of the vortex structure. The collapse and formation of the stratified dipolar structure is detailed in the study of Flór & van Heijst (1994).

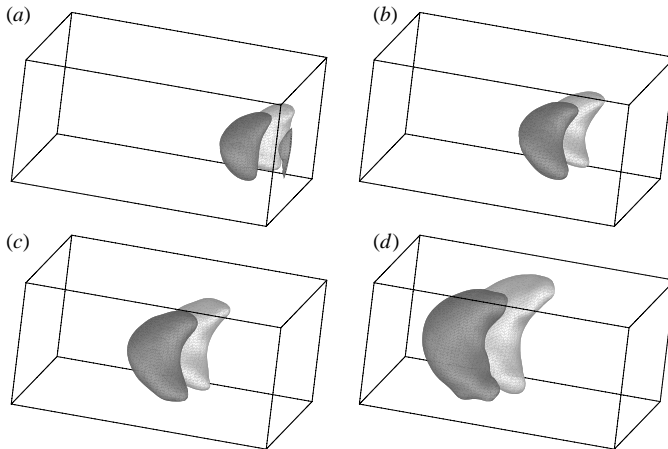


FIGURE 2. Isosurface of ω_z inside the core for $|\omega_z| = 15\%$ of the maximum value of ω_z at $t = 630, 1150, 1780$ and 3140 s after the injection. Positive ω_z is in dark grey and negative is in light grey. The dipole is propagating to the left. The size of the domain represented is $200 \times 160 \times 30$ cm and the vertical axis has been stretched by factor 4 to enhance the visualization.

Once formed, the dipolar vortex structure translates quasi-steadily along a straight trajectory (if symmetric) away from the injector. The Reynolds number based on the injection parameters, Re_i , has a typical value of 15000. Soon after the dipole formation is completed, the Reynolds number based on the horizontal characteristics of the structure, $Re = UL_h/\nu$, is typically $O(1000)$. This value decreases rapidly as the dipole decays during the course of the experiment.

The three-dimensional structure of the dipole is examined in figure 2. Although the motion is quasi-horizontal, the vortical structure is definitely not two dimensional. The vertical vorticity is bent backward behind the dipole due to the vertical variability in the propagation speed, which must go to zero far above and below the structure and is maximum at the mid-plane. This self-advective deformation gives each half of the dipole a ‘banana’-like appearance. This three dimensional structure of the dipole was previously observed in the experiments of Fincham (1998, 2000). Full three-dimensional numerical simulations of the interaction of two shielded monopoles in a stratified fluid also exhibit this characteristic banana shape (Beckers *et al.* 2002).

4.2. Vertical structure and aspect ratio

The vertical structure of the dipole is examined by considering the vertical distribution of the vertical vorticity along the banana shape. The maximum value of ω_z following this deformed vortex tube, $\omega_{z,max}$, is plotted versus the vertical coordinate in figure 3. The vertical distribution of $\omega_{z,max}$ is approximated well by a Gaussian of the form $\exp(-(z - z_0)^2/\sigma^2)$, where z_0 is the altitude of the mid-plane and σ is a measure of the dipole thickness. σ obtained in this way is similar to a σ obtained by simply fitting ω_z in z , as the advection-induced deformation is minimum at the centreplane where ω_z is maximum. Such Gaussian distributions seems to be general properties of isolated structures in stratified fluids and this measure of σ is used throughout the study. Similar distributions were indeed observed for decaying dipolar vortices (Flór & van Heijst 1994; Flór *et al.* 1995) and decaying monopoles (Beckers *et al.* 2001).

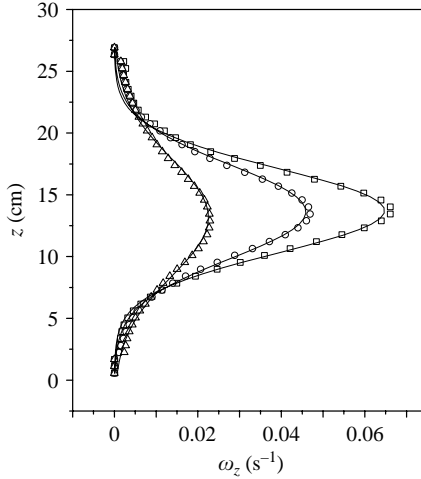


FIGURE 3. Vertical distribution of $\omega_{z \max}$ following the deformed tube of vertical vorticity at: \square , $t = 360$ s; \circ , $t = 620$ s; \triangle , $t = 1350$ s after injection. The measured profiles are fitted with Gaussian curves. $V = 0.54$ l, $\delta t = 3$ s.

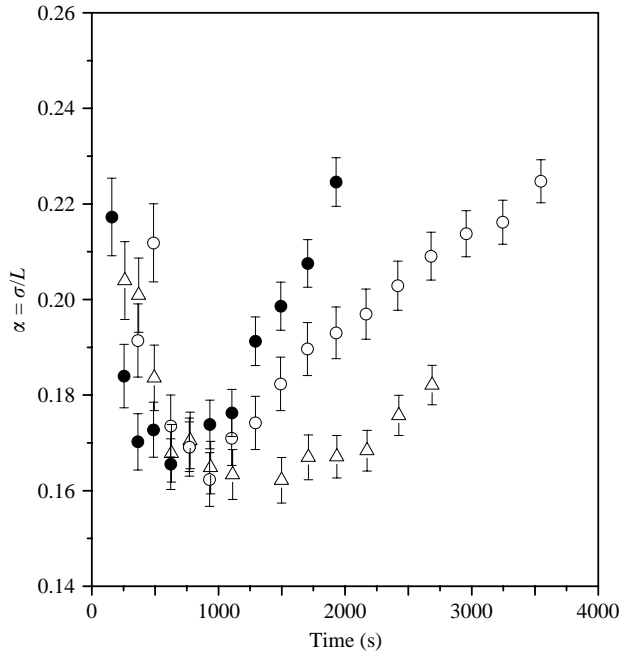


FIGURE 4. Evolution of the aspect ratio, $\alpha = \sigma/L_h$, for three dipoles: \triangle , $V = 0.60$ l; $\delta t = 3$ s; \circ , $V = 0.68$ l, $\delta t = 4$ s; \bullet , $V = 0.54$ l, $\delta t = 3$ s.

The evolution of the aspect ratio $\alpha = \sigma/L_h$, where L_h is the distance between the vortex poles, is illustrated in figure 4. Two regimes can be defined. For early times a decrease of the aspect ratio is observed. This regime corresponds to an advective regime in which horizontal advection dominates, deforming the dipole, bending the vertical vorticity horizontally and thinning the dipole as fluid is stripped off in the high-shear regions above and below, while the horizontal size of the structure grows

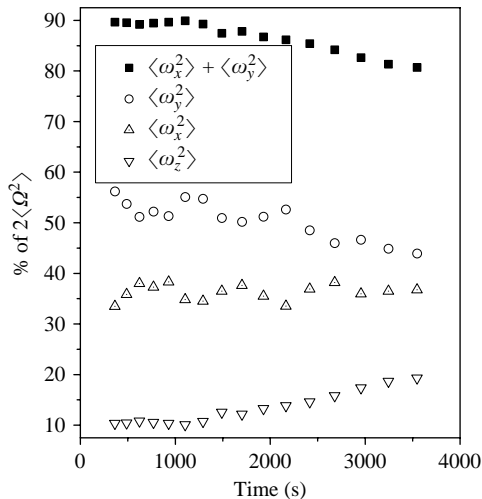


FIGURE 5. Contribution of the three components (ω_x , ω_y , ω_z) of vorticity to the total enstrophy Ω . $V = 0.541$, $\delta t = 3$ s.

by viscous entrainment of the ambient fluid. For later times, a second regime where α increases by vertical diffusion is observed. In this regime, the rate of the vertical expansion by diffusion is larger than the horizontal expansion rate. As we shall see in §6, the transition time between the two regimes is governed by an effective Reynolds number, which measures the relative importance of the horizontal inertial forces to the vertical viscous diffusion.

This second regime, where the thickness grows much more rapidly than the horizontal scale corresponds to the regime observed and described by Flór & van Heijst (1994) and Flór *et al.* (1995). The values of the aspect ratio of the dipole are consistent with the observations of pancake eddies in stratified flows. For example, in the wake of a sphere, Bonnier *et al.* (2000) measured $\alpha \sim 0.4$ and Spedding (2002) measured $\alpha \sim 0.3 - 0.6$; Fincham *et al.* (1996) measured $\alpha \sim 0.3$ for late-time stratified turbulence, and for the vortex dipole, Voropayev *et al.* (1995) find $\alpha \sim 0.4$, whereas Flór *et al.* (1995) find $\alpha \sim 0.2 - 0.4$. The differences in the observed values of α can be attributed to a number of things, including errors in the different measurement techniques used and the stage of development that the vortex is in. The actual definition of the length scales is not always the same: some are based on fits to vorticity profiles, others on fits of velocity or scalar fields, and multipolar vortices do not always have easily definable horizontal scales. Most importantly, it is the initial conditions responsible for the generation of the vortices and the ambient conditions of the environment they develop in that determines α .

4.3. Vortex filaments

This low-aspect-ratio characteristic of late-time vortical structures in stratified fluids indicates a strong anisotropy of the flow and, thus, a relatively large difference in intensity between the horizontal and vertical velocity gradients. As it can be seen in figure 5, the horizontal vorticity is responsible for about 90% of the total enstrophy, with ω_y , here composed entirely of $\partial u / \partial z$, contributing more than 50%.

The importance of the vertical gradients is illustrated well in figure 6 which displays the topology of the vortex lines within the dipole core (see Fincham *et al.* 1996; Fincham 1998, 2000). Because of up-down symmetry about the horizontal mid-plane,

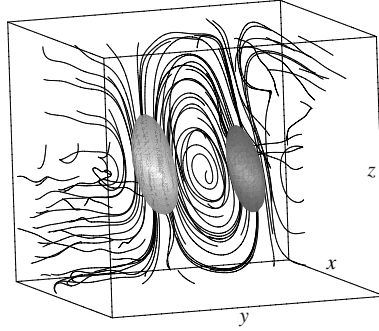


FIGURE 6. Vortex filaments originating from a vertical plane traversing the dipole. The vertical axis has been stretched four times.

the vortex lines must be directed vertically on the central horizontal plane where the vertical vorticity has its maximum value. The lines clearly exhibit a tendency to form closed vortex loops and connect the two poles of the dipole through regions of strong horizontal vorticity (it should be noted that the vortex filaments never actually close on themselves, rather they continue to loop around endlessly in a somewhat chaotic way). Away from the core of the structure the topology of the vortex filaments is more complicated. The DNS of Gourlay *et al.* (2001) shows similar vortex line topology for stratified wake vortices, that can be considered as an array of joined dipoles as proposed by Spedding *et al.* (1996).

The horizontal vortex sheets observed below and above the core of the dipolar structure are associated with high-shear regions in which the kinetic energy, entirely contained in the quasi-horizontal motion, is dissipated. This idea of highly dissipative horizontal vortex sheets that can connect the neighbouring structures was expressed by Fincham *et al.* (1996) to explain the organization of patches of vertical vorticity observed in stratified turbulence experiments. In their study they also observed that 90% of the kinetic energy is dissipated by these sheets of horizontal vorticity.

From these considerations, we define an effective Reynolds number, based on the horizontal inertial forces and the vertical dissipative shearing:

$$Re_{eff} = \frac{\text{inertial force}}{\text{viscous force}} = \frac{U^2/L_h}{\nu U/\sigma^2} = \frac{\sigma^2}{L_h^2} Re$$

or

$$Re_{eff} = \alpha^2 Re \quad (4.1)$$

where Re is the horizontal Reynolds number ($Re = UL_h/\nu$). Due to the strong anisotropy of the flow, the effective Reynolds number, Re_{eff} , is reduced by a factor α^2 relative to the horizontal Reynolds number. The importance of this effective Reynolds number will be discussed in § 6.

5. Comparison: experiment and quasi-horizontal model

5.1. Model initialized with experimental data

Here we compare some measured characteristics of the dipolar vortices to the result of numerical simulations of the reduced equation (3.5). In order to have an exact comparison between the experiments and the model, the numerical calculation is initialized with the three-dimensional experimental data. The initial condition of the

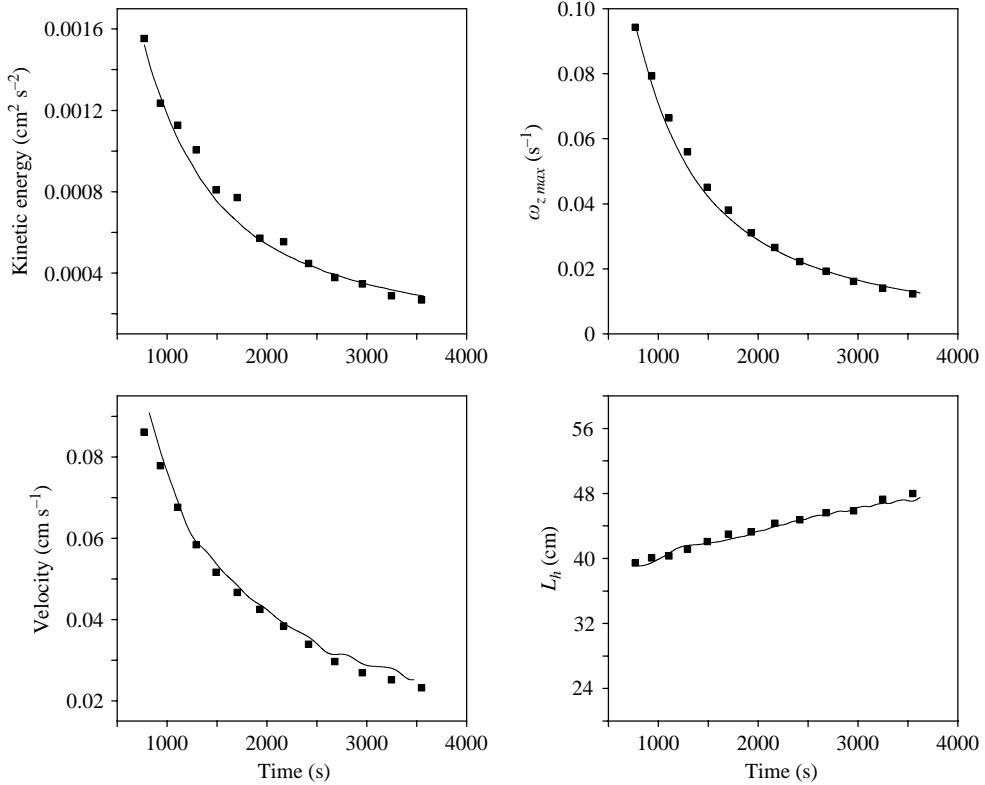


FIGURE 7. Comparison of the evolution of some characteristics of the dipolar structure (kinetic energy, maximum vertical vorticity, translation velocity and distance between the two poles) between experiment (black squares) and numerical simulation initialized with the first measured vertical vorticity field (solid line). $V = 0.68l$, $\delta t = 4$ s.

flow is defined by the measured vertical vorticity field soon after the collapse of the turbulent patch, just after its reorganization into quasi-horizontal motion.

Results of this simulation are compared with the experimental data in figure 7. The evolution of kinetic energy, maximum vertical vorticity, translation velocity and distance between the two poles are all in very good agreement. The distance between the poles shows a relatively linear growth with time, similar to that found by Flór & van Heijst (1994).

Based on the principle of conservation of momentum and the entrainment of ambient fluid Voropayev *et al.* (1991) derived an expression for the dipole characteristics and their evolution soon after formation. For the experiment shown in figure 7, at $t = 750$ s, their estimates yield $L = 45$ cm, $U = 0.09$ cm s $^{-1}$ and $\sigma = 45$ cm. The agreement is fairly good for the horizontal size and the translation velocity of the dipole. However, their prediction exaggerates significantly the value of σ observed in the present experiments ($\sigma \sim 12$ cm). It should be noted that their definition of σ is based on the vertical profile of horizontal velocity, which for the dipoles studied here, tends to give values for σ about 30% larger than that from the profiles of vertical vorticity. For the very large forcing considered here, the effect of mixing, which is not considered in their analysis, cannot be neglected. In addition, during the formation process, the vertical shear is initially very large, and tends to wash out the bottom and

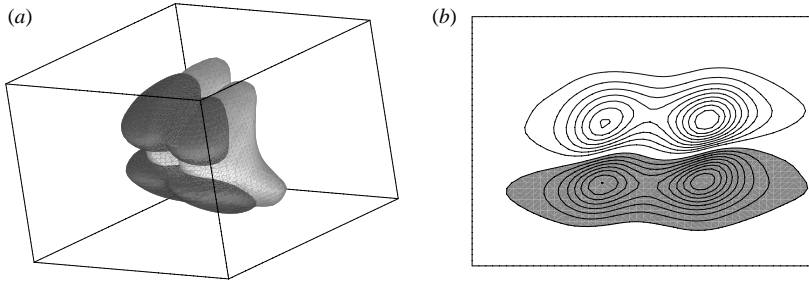


FIGURE 8. (a) Isosurface of ω_z (in light grey) and of the density perturbation ρ (in dark grey) for 15% of their maximum value. (b) Isolines of the density perturbation in a vertical plane through the dipolar vortex core. The positive part of ρ is in dark grey, while the negative part is in white. Contour interval $\Delta\rho = 1.3 \times 10^{-5} \text{g cm}^{-3}$.

upper part of the structure leading to a thinner dipole. A detailed analysis of the effect of vertical shear on a dipole can be found in Voropayev, Smirnov & Brandt (2001).

This agreement between the numerical simulation and the experiments shows that, for the present flow conditions, the observed dipolar vortex structure can be characterized as a stack of quasi-independent two-dimensional coherent vortices vertically coupled by viscosity, as proposed for stratified turbulence by Lilly (1983). An important factor in the model is its complete independence from the level of the stratification. However, this model, which is suitable for describing the viscous decay of any isolated structure, is valid only in the low-Froude-number hypothesis $Fr_v \ll 1$ and in the absence of internal gravity waves.

For an isolated decaying monopolar vortex, comparisons of full three-dimensional numerical simulations of the Boussinesq equations with an analytical model, based on an exact resolution of (3.5), performed by Beckers *et al.* (2001), shown that for $Fr_v \ll 1$, (3.5) is sufficient to describe the evolution of the structure. In this regime, the decay is also found to be independent of the stratification. However, for larger vertical Froude number, $Fr_v > 1$, they observed departures from this model. These departures, including vertical velocities associated with a recirculation, are second-order effects ($O(Fr_v^2)$) and remain of limited importance in the regime we investigate here.

In view of the close agreement between the experiments and the model, detailed information, which cannot be easily measured during the experiments, such as the three-dimensional fields of pressure and density fluctuations, can be obtained respectively from the numerical resolution of (3.6) and (3.3). The density perturbation field, $\rho(x, y, z)$, associated with the dipolar structure is represented together with the vertical vorticity in terms of an isosurface in figure 8. As can be seen in figure 8, the upper part of the structure exhibits a weaker density than the ambient stratification while the lower part exhibits a stronger density. The maxima of the deviations are observed above and below the centre of each pole. This pinching of the isopycnals above and below each pole has the effect of increasing the local value of the Brunt-Väisälä frequency N by as much as 2 times on the centreplane. Correspondingly the value of N at $z = \pm\sigma/\sqrt{2}$ is significantly reduced. As $z = \pm\sigma/\sqrt{2}$ also corresponds to zones of maximum vertical shearing, we would expect to find the minimum Richardson number here. The minimum Richardson number was found to be consistently larger than 0.25 even for the earliest times measured, a result consistent with the findings of Bonnier *et al.* (2000), suggesting that in the process of vortex formation, any critical regions are quickly ‘diffused’ by the associated turbulence.

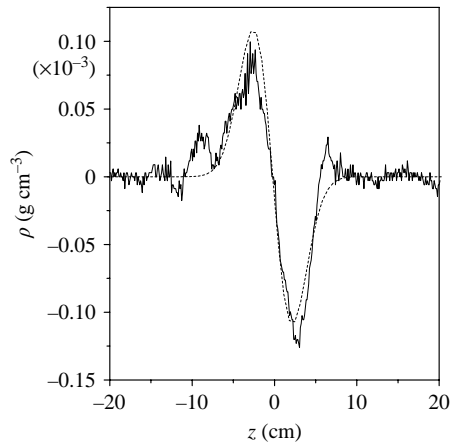


FIGURE 9. Measured profile of density perturbation relative to undisturbed fluid through the center of one pole (solid line) and obtained from the vertical vorticity field using the cyclostrophic and hydrostatic assumptions (dashed line).

At early times, the available potential energy contained in the density perturbation field represents less than 3% of the total kinetic energy of the structure. This potential energy is released gradually during the decay of the structure and has the effect of stretching the vertical vorticity as the pinched isopycnals return to their horizontal rest state. Vortex stretching, which was reported and discussed by Beckers *et al.* (2001), corresponds to a conversion of potential energy stored in the deformation of the isopycnals into kinetic energy of the vortex. This process is associated with a secondary circulation in which a radially inward flow takes place inside each pole of the dipole. This process, which can affect the decay and the growth of the vortex, cannot be described by the set of equations (3.1)–(3.4). Nevertheless, because it remains a $O(Fr_v^2)$ effect, this process does not significantly affect the decay of the dipolar vortex in the regime we investigate.

A comparison between the density obtained from the vertical vorticity field and that measured directly by a conductivity probe is shown in figure 9, where the profile is measured through the centre of one pole. The good agreement confirms the validity of the cyclostrophic balanced state model proposed by Bonnier *et al.* (2000) and Beckers *et al.* (2001, 2002). These authors, along with Voropayev *et al.* (1991), have made similar density profile measurements of late-time stratified vortices.

5.2. Three-dimensional extension of the Lamb–Chaplygin dipolar vortex

To investigate the role of the Reynolds number and the initial dipole thickness, and to better understand the processes that govern the evolution of the dipole, numerical simulations of the evolution of the collapsed structure were done. Here we describe a simple model for a three-dimensional dipole that is consistent with the experimental observations. Many sophisticated approaches to using classical flow solutions to help characterize the evolution of real flows have been developed: see Turner (1964) for the flow into an expanding spherical vortex and Voropayev *et al.* (1991) for flow into an expanding planar dipole. Here, the flow solution is used only as an initial condition for the numerical simulations and the approach is kept simple.

Flór & van Heijst (1994) and Flór *et al.* (1995) have shown that a planar dipole generated by a turbulent injection can be described well by a theoretical model called the Lamb–Chaplygin dipole. This model for a two-dimensional dipolar vortex with

continuously distributed vorticity on a circular area was first described by Lamb (1932) and later by Batchelor (1967). A similar, more general dipole solution was formulated independently by Chaplygin in 1902, see Meleshko & van Heijst (1994) and is referred to in this paper as the Lamb–Chaplygin dipole. Lamb and Chaplygin proposed a localized solution of the two-dimensional Euler equations where

$$\omega_z = \begin{cases} \lambda^2 \psi', & r \leq R_0 \\ 0, & r > R_0. \end{cases} \quad (5.1)$$

λ is a constant, ψ' the streamfunction in the frame of reference moving with the dipole and R_0 the radius of the dipole. The Lamb–Chaplygin dipolar solution in the frame moving with the dipole is given by:

$$\psi'(r, \theta) = \begin{cases} -\frac{2UR_0}{\gamma J_0(\gamma)} J_1(\lambda r) \sin(\theta), & r \leq R_0 \\ U \left(\frac{R_0^2}{r} - r \right) \sin(\theta), & r > R_0, \end{cases} \quad (5.2)$$

with U the dipole's translation speed, (r, θ) the cylindrical coordinates in the horizontal plane (θ is measured from the dipole axis), and J_0 and J_1 the Bessel functions of zero and first order. Continuity of the velocity at $r = R_0$ requires $\lambda R_0 = \gamma$ where $\gamma = 3.8317$ is the first zero of J_1 .

To compare the measured horizontal distribution of vertical vorticity ω_z to this solution, we calculate the streamfunction ψ' for several different horizontal planes. The streamfunction ψ in the laboratory frame is obtained by solving $\nabla_h^2 \psi = -\omega_z$. We then obtain $\psi'(x, y, z)$ by applying the transformation $\psi'(x, y, z) = \psi(x, y, z) - U_x(z)y + U_y(z)x$, where U_x and U_y are the components of the dipole's translation velocity.

Figure 10 shows the horizontal distribution of ω_z and the streamfunction ψ' in two different horizontal slices of the laboratory-generated dipole and the associated scatter plots $\omega_z = f(\psi')$. On these plots the points collapse quite well onto a single curve with two branches. The points clustered in the horizontal band with $\omega_z = 0$ correspond to the potential flow outside the dipole, while the others are associated with the rotational flow inside the dipole. This behaviour indicates that the flow in each level z is almost a stationary state of the two-dimensional Euler equation.

The curve $\omega_z = f(\psi')$ shows a slightly nonlinear relationship, with a sinh-like profile. A similar nonlinear profile was also observed in experiment and numerical simulation (Couder & Basdevant 1986; Nguyen Duc & Sommeria 1988; Flór & van Heijst 1994; Beckers *et al.* 2002). Flór & van Heijst (1994) noticed that dipoles created by the collapse of a turbulent jet always exhibit such a nonlinear (ω, ψ') relationship whereas dipoles generated from a laminar injection exhibit a much more linear (ω, ψ') relationship. Similar results were obtained by Beckers *et al.* (2002) who observed that the deviation from the linear relationship increases with the Reynolds number. A common result of these observations is that this nonlinear profile is associated with a relatively weak linking of the dipole's constituent vortices. For a dipole generated by turbulent injection, the viscous entrainment of nearly irrotational fluid into the dipole tends to increase the separation of the vortex centres and thus leads to a less compact structure.

Although the (ω, ψ') relationship is not linear these curves can still be reasonably well fitted to a linear function $\omega_z = \lambda^2 \psi'$ at all z . The slope, λ^2 , obtained from a linear least square fit of points having non-zero vorticity in figure 10 remains the same for the

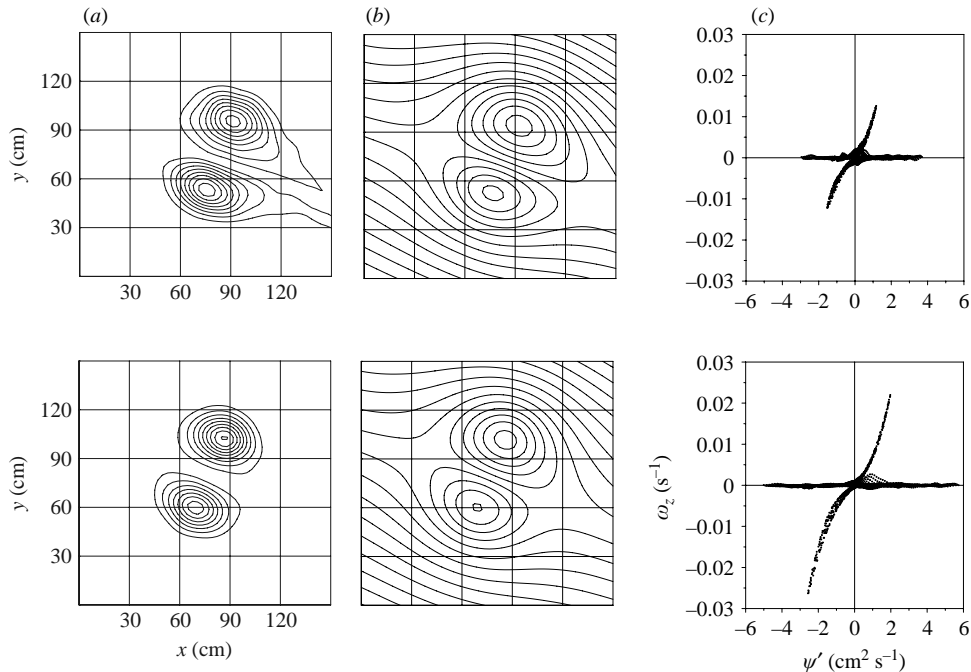


FIGURE 10. (a) Horizontal distribution of the vertical vorticity, ω_z . (b) Streamfunction, ψ' , in the frame of reference translating with the planar dipole. (c) Scatter plot of the relation $\omega_z = f(\psi')$; $z = +3/4\sigma$ cm and $z = 0$ cm. The dipole is propagating to the left and up.

different z , $\lambda^2 = (8.9 \pm 0.2) \times 10^{-3}$. This estimation corresponds well with the value of $\lambda^2 = (9.0 \pm 0.1) \times 10^{-3}$ obtained with the relation $\lambda^2 = (\gamma/R_0)^2$ for a Lamb–Chaplygin dipole with a radius R_0 equal to that measured from the contour plots in figure 10. Moreover, the radius of the dipole remains the same along the tube of vertical vorticity; only its strength changes (figure 3). We thus consider as a model for the initial three dimensional dipole a vertical assembly of similar planar Lamb–Chaplygin dipoles, with strengths vertically distributed according to a Gaussian curve, $\exp(-z^2/\sigma^2)$. Even without viscosity, this three-dimensional model is not stationary. Due to the vertical variability of the self-advection, a deformation of the structure will occur.

According to the model developed above, the dipole is characterized by three quantities: its radius R_0 , its translation velocity U and its vertical extent, σ . The values of R_0 and U are taken to be 1, as they are non-dimensional variables. The free parameters are the horizontal Reynolds number, Re , and σ . So, given the Reynolds number, the effective Reynolds number, defined by (4.1), is directly determined by the choice of σ . For a specific case, $Re = 1000$ and $\sigma = 0.2$, the evolution and the three-dimensional structure of the flow obtained from the numerical simulation are illustrated in figure 11. Good qualitative agreement with the experiments represented in figure 2 can be seen.

When comparing results from the laboratory experiments and the numerical simulations, it is important to account for the different time origins and initial conditions. The simulations are initialized at time t_0 , with a collapsed structure that undergoes an initial reorganization. In the experiments, t_0 corresponds to the end of the injection process. Typically, the collapse is mostly completed in about 15 buoyancy periods or approximately 315 s, at which point the data acquisition is started. A time

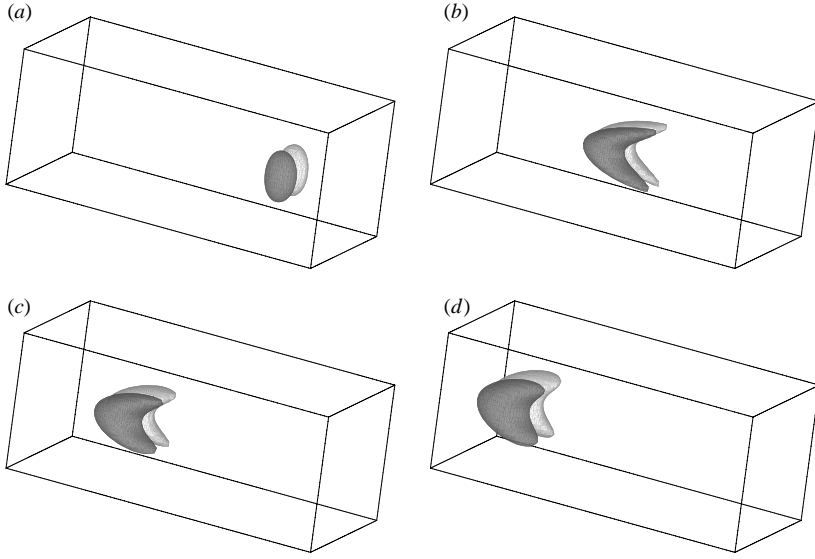


FIGURE 11. Isosurface of ω_z inside the core for $|\omega_z| = 15\%$ of the maximum vertical vorticity from the numerical simulation at $t = 0$, $t = 5$, $t = 10$, $t = 15$ ($Re = 1000$, $\sigma = 0.2$). The vertical axes have been stretched by factor 4 to enhance the visualization.

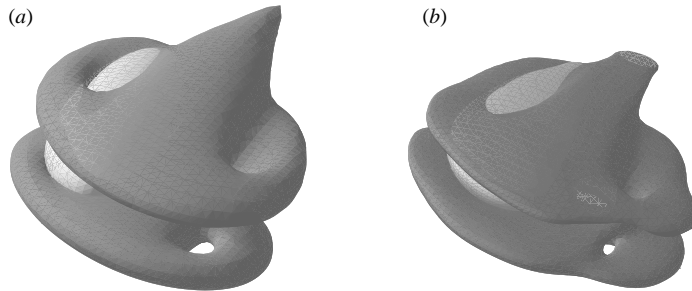


FIGURE 12. Isosurfaces of enstrophy (dark grey) for 20% of the maximum and negative ω_z (light grey) for 15% of the minimum. Numerical simulation (a) and experiment (b).

scale can be defined from the speed and horizontal size of the measured structure in the first volume acquired. Using this normalization, the non-dimensional computational time units correspond to roughly 350 s each.

Figure 12 shows a comparison between the enstrophy fields of the simulated and experimentally measured dipoles for approximately similar non-dimensional times. In both cases two horizontal sheets of strong horizontal vorticity can be seen sandwiching the dipole core; the holes, representing local minima in the enstrophy field, correspond approximately to zero-velocity regions in the laboratory reference frame and are located slightly in front and to the outside of the deformed cores of the vertical vorticity structure.

6. Horizontal advection–vertical diffusion balance

The effect of the initial horizontal Reynolds number and effective Reynolds number on the decay of the dipolar vortex is illustrated in figure 13. The decay of the total

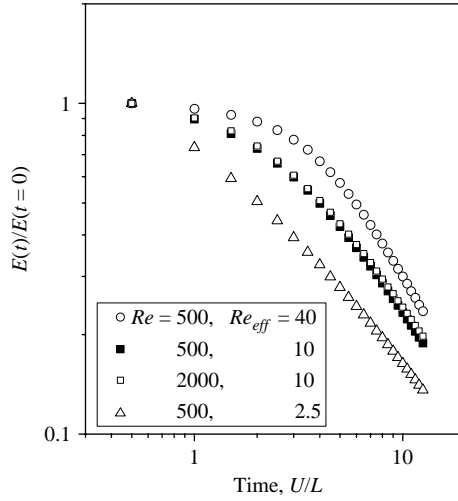


FIGURE 13. Decay of the normalized kinetic energy of the dipole from the numerical simulation for four different initial conditions. This graph shows that the decay is governed by Re_{eff} .

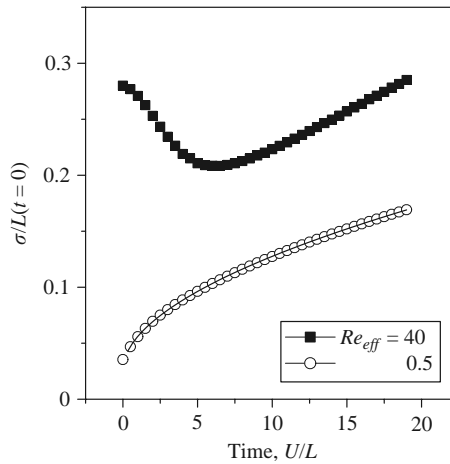


FIGURE 14. Evolution of the vertical length scale of the dipole for two different values of the initial Re_{eff} , both with $Re = 500$. The solid line shows a growth according to a diffusing process \sqrt{t} .

kinetic energy is directly related to the effective Reynolds number. The two simulations with the same $Re_{eff} = 10$ exhibit exactly the same decay, yet they were initialized with vastly different horizontal Reynolds numbers (500 and 2000). The energy decay is thus governed by the effective Reynolds number, which is consistent with the experimental observations showing that the kinetic energy is almost entirely dissipated through the vertical gradients.

Moreover, as can be seen in figure 14 two different initial behaviours of the dipole thickness are observed depending of the initial value of Re_{eff} . For small initial Re_{eff} (thin dipole), the vertical length starts to grow, whereas for large initial effective Reynolds number the vertical scale starts to decreases until it reaches its minimum value and then increases monotonically with time. In the first case, diffusion is

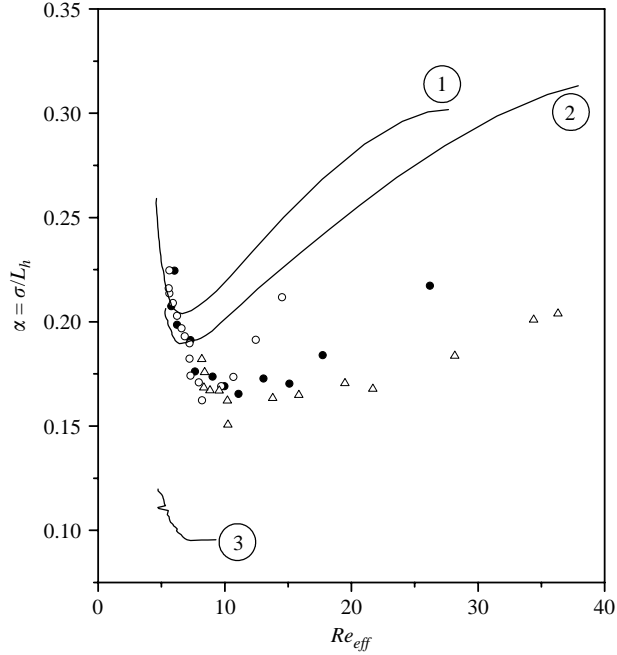


FIGURE 15. Evolution of the aspect ratio α as a function of Re_{eff} , for numerical simulation (solid line) with different initial horizontal Reynolds numbers of: curve 1, 350; 2, 500; and 3, 2000. From experiments: Δ , $V = 0.60$ l, $\delta t = 3$ s; \circ , $V = 0.68$ l, $\delta t = 4$ s; \bullet , $V = 0.54$ l, $\delta t = 3$ s.

dominant over advection, the evolution is purely diffusive and the thickness grows according to \sqrt{t} . This regime correspond to the regime previously observed and described by Flór *et al.* (1995). In the second case, Re_{eff} is initially large and the dynamics is dominated by the horizontal advection. High-shear regions confine the dipole, acting as boundaries between the moving dipole core and ambient fluid above and below. As the dipole advances the lower and upper boundaries tend to be washed away, thinning the structure. This process is enhance by the ongoing self-induced deformation which increases the importance of vertical shear. All this contributes to a decrease of σ . During this process, the temporal effective Reynolds number decreases until it reaches a critical value coinciding with the minimum value of σ . Thereafter diffusion overwhelms advection and the vertical scale starts growing with \sqrt{t} .

Similar behaviour of σ was observed by Godoy-Diana, Chomaz & Billant (2003) for initially tall dipoles and a mechanism of ‘viscous peel-off’ was proposed to explain the evolution of the thickness of the structure. This model, also based on an advection–vertical diffusion balance predicts that σ should decreases until it reaches a ‘viscous scale’, $\delta = L_h Re^{-1/2}$. The time needed for the vertical scale to reach δ , estimated from figure 14, is $T_c = 6.5$. This estimate is in very good agreement with their model, which predicts $T_c = \alpha_0 Re^{1/2} L_h / U = 6.3$ (using $U = 1$, $L_h = 1$, $Re = 500$ and $\alpha_0 = 0.28$).

The two different evolutionary regimes of the dipolar structure observed in figure 4 are directly related to the value of the effective Reynolds number; this is illustrated in figure 15 which shows the evolution of the aspect ratio of the structure as a function of the time-dependent Re_{eff} . The time evolution is from right to left. In all cases we observe the two regimes. For early times, when Re_{eff} is large compared to unity, α decreases; this corresponds to the advective regime. This regime, which

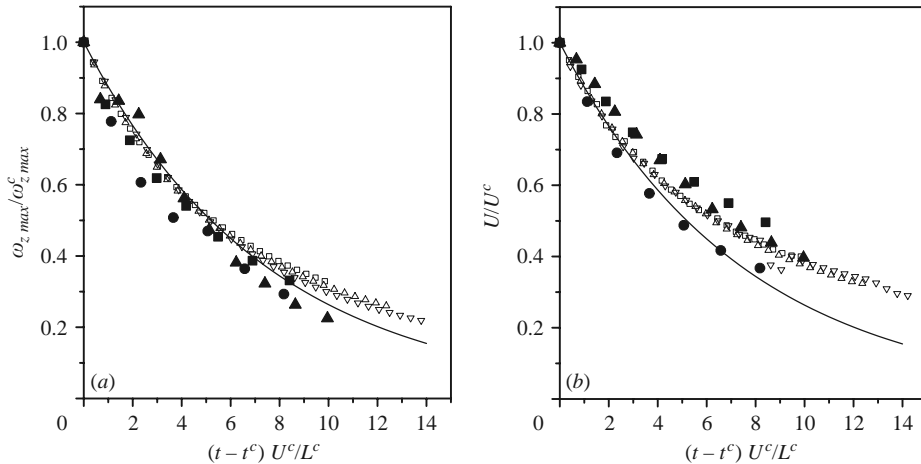


FIGURE 16. Time evolution of the maximum value of (a) the vertical vorticity and (b) the translation velocity of the dipole for both experiments (black symbols) and numerical simulation (open symbols) after the transition to the diffusive regime. The curves are normalized by their value at the transition and the time is scaled by the advective time scale at this transition. The solid line is an exponential decay with e-folding time Re_{eff}^c .

cannot be described by the usual diffusion model, persists until Re_{eff} reaches the critical value, Re_{eff}^c , which corresponds to a balance between horizontal advection and vertical diffusion. The critical value at which the transition occurs is independent of the initial condition and confirms that for initially large Re_{eff} , the aspect ratio of the dipole decreases down to $\alpha \sim Re^{-1/2}$ as predicted by Godoy-Diana *et al.* (2003). For later times, the structure enters the diffusively dominated regime, and we observe the inverse phenomena, α increases, while the effective Reynolds number remains almost constant.

Since the only relevant parameter is the effective Reynolds number, soon after the transition, the dipolar vortex should develop a self-similar regime. Scale U , L and σ by their value at the transition, U^c , L^c and σ^c , and define the dimensionless advective time $(t - t^c)U^c/L^c$ where t^c is the transition time. The temporal evolution of the maximum value of the vertical vorticity and the translation velocity after the transition are shown in figure 16. In both graphs the curves collapse fairly well indicating a self-similar decay which is independent of the initial conditions. In this regime, the evolution is compared with the ‘constant thickness’ model proposed by Flór *et al.* (1995) (solid line in figure 16) which gives, on short time scales, a useful approximation of the viscous decay of the dipolar vortex. According to this model, the decrease of the maximum value of the vertical vorticity and of the translation velocity occurs on a time scale $\tau \sim \nu^{-1}\sigma$ which corresponds to a dimensionless decay time Re_{eff}^c . For larger times, the approximation of constant thickness is no longer valid. A more complete model which accounts for the vertical expansion Flór *et al.* (1995) using combined algebraic and exponential decay could then be used.

7. Conclusion

Experiments on the three-dimensional structure of a stratified vortex dipole were performed at large scale and for moderate Reynolds numbers in the low-Froude-number regime. These experiments were accompanied by corresponding numerical

and theoretical investigations under the low-Froude-number hypothesis $Fr_v \ll 1$. The novel measurement technique used, provided access to the three dimensional structure of the vorticity field and permitted the assimilation of the data into the numerical model. Such low-Froude-number coherent structures are described well by a simple model based on the horizontal advection of the vertical vorticity (z -dependent) where the different layers are coupled only by viscosity. Although the dynamics are controlled by the horizontal velocity field, the diffusion is mainly in the vertical direction. The experiments revealed the self-induced banana-like structure of the vertical component of vorticity and the tendency of the vortex lines to form closed loops in the dipole core. The quasi-three-dimensional model exhibited excellent agreement with the experimental data when initialized with a measured vorticity field. This agreement was good for both the time evolution of average basic quantities, such as the energy and vertical vorticity, as well as for the evolution of the translation velocity and the distance between the poles. However this model is not able to capture $O(Fr_v^2)$ effects such as the secondary recirculation that may influence the dynamic of the structure as observed by Beckers *et al.* (2001) for the decay of a monopolar vortex. Thus, even though if the basic mechanisms are captured by this model, full three-dimensional simulation will be needed to investigate the initial regime $Fr_v \sim O(1)$.

The model also permitted the evaluation of additional quantities that were not accessible experimentally, such as the density and pressure fields corresponding to the experimental velocity data. Density measurements through one of the poles were in excellent agreement with that predicted by the model. This good agreement led to the development of a fully three-dimensional stratified Lamb–Chaplygin dipole model, which was used as an initial condition, allowing the simulation of higher Reynolds number dipoles. The observation that almost all of the energy dissipation is by vertical shearing of the horizontal velocity field suggested the introduction of an effective Reynolds number based on horizontal inertia and vertical diffusion. This effective Reynolds number was shown to govern the overall decay of the dipole and to define two regimes. If $Re_{eff} \ll 1$ the evolution is purely diffusive while for large Re_{eff} , the dipole undergoes an advectively driven thinning process until $Re_{eff} \sim O(1)$. Then, diffusion becomes the dominant process and the evolution, which is independent of the initial conditions, is predicted well by an exponential decay with a decay time given by Re_{eff}^{ϵ} .

Dipolar vortices occurring at geophysical scales, where the Reynolds numbers are many orders of magnitude larger than those studied here, are believed to exhibit similar dynamics. At these high Reynolds numbers, the molecular viscosity would be replaced by an effective turbulent viscosity. Due to strong natural forcing and interactions with other vortices (that can dramatically increase the vertical shearing) these dipoles cannot be considered as freely decaying and it is expected that the shear layers confining these geophysical structures would become unstable (as shown, the density field perturbations associated with the dipolar structure produce minimum stratification in the regions of maximum vertical shearing). Instability of these shear layers will have the effect of locally increasing the effective turbulent eddy viscosity, compensating for any increased shearing, hence restoring the advective–diffusive balance. However, in geophysical flows, internal gravity waves cannot always be neglected as in the present model and a description of their interactions with the coherent structures would be useful to achieve a better understanding of these vortices at geophysical scales.

These laboratory experiments would not have been possible without the support of Dr Henri Didelle, Dr Dominique Renouard and Mr René Carcel.

REFERENCES

- BATCHELOR, G. K. 1967 *An Introduction to Fluid Dynamics*. Cambridge University Press.
- BECKERS, M., CLERCX, H. J. H. & VAN HEIJST, G. J. F. 2002 Dipole formation by two interacting shielded monopoles in a stratified fluid. *Phys. Fluids* **14**, 704–720.
- BECKERS, M., VERZICCO, R., CLERCX, H. J. H. & VAN HEIJST, G. J. F. 2001 Dynamics of pancake-like vortices in a stratified fluid: experiments, model and numerical simulations. *J. Fluid Mech.* **433**, 1–27.
- BILLANT, P. & CHOMAZ, J. 2000 Theoretical analysis of the zigzag instability of a vertical columnar vortex pair in a strongly stratified fluid. *J. Fluid Mech.* **419**, 22–63.
- BILLANT, P., CHOMAZ, J. & HUERRE, P. 2000 Experimental evidence for a new instability of a vertical columnar vortex pair in a strongly stratified fluid. *J. Fluid Mech.* **418**, 167–188.
- BONNIER, M. 1999 Sillage d'une sphère en milieu linéairement stratifié. Caractérisation des structures tourbillonnaires. PhD, Institut National Polytechnique de Toulouse, Toulouse, France.
- BONNIER, M., EIFF, O. & BONNETON, P. 2000 On the density structure of far-wake vortices in a stratified fluid. *Dyn. Atmos. Oceans* **31**, 117–137.
- CHOMAZ, J. M., BONNETON, P., BUTET, A. & HOPFINGER, E. J. 1993 Vertical diffusion of the far-wake of a sphere moving in a stratified fluid. *Phys. Fluids A* **5**, 2799–2806.
- COUDER, Y. & BASDEVANT, C. 1986 Experimental and numerical study of vortex couples in two dimensional flows. *J. Fluid Mech.* **173**, 225–251.
- EMBED, P. & MAJDA, A. 1998 Low Froude number limiting dynamics for stably stratified flows with small or finite Rossby numbers. *Geophys. Astrophys. Fluid Dyn.* **87**, 1–50.
- FEDOROV, K. & GINSBURG, A. 1989 Mushroom-like currents (vortex-dipoles): one most widespread form of non-stationary coherent motions in the oceans. In *Mesoscale/Synoptic Coherent Structures in Geophysical Turbulence* (ed. J. C. J. Nihoul & B. M. Jamart), pp. 1–14. Elsevier.
- FINCHAM, A. M. 1994 The structure of decaying turbulence in a stably stratified fluid: Measurements with a novel digital particle imaging velocimetry system. PhD, University of Southern California, Aerospace Engineering, Los Angeles, USA.
- FINCHAM, A. M. 1998 3D measurement of vortex structures in stratified fluid flows. *Proc. IUTAM Symp. Simulation and Identification of Organized Structures in Flows* (ed. J. N. Soerensen, E. J. Hopfinger & N. Aubry), pp. 273–287. Kluwer.
- FINCHAM, A. M. 2000 Coherent vortex structures in stably stratified rotating fluids. *Proc. IUTAM Symp. Developments in Geophysical Turbulence* (ed. R. M. Kerr & Y. Kimura), pp. 193–203. Kluwer.
- FINCHAM, A. M. & DELERCE, G. 2000 Advanced optimization of correlation imaging velocimetry algorithms. *Exps. Fluids* **29**, S13–S22.
- FINCHAM, A. M., MAXWORTHY, T. & SPEDDING, G. R. 1996 Energy dissipation and vortex structure in freely decaying stratified grid turbulence. *Dyn. Atmos. Oceans* **23**, 155–169.
- FINCHAM, A. M. & SPEDDING, G. R. 1997 Low cost, high resolution DPIV for measurement of turbulent fluid flow. *Exps. Fluids* **23**, 449–462.
- FLÓR, J. B. & VAN HEIJST, G. J. F. 1994 An experimental study of dipolar vortex structures in a stratified fluid. *J. Fluid Mech.* **279**, 101.
- FLÓR, J. B., VAN HEIJST, G. J. F. & DELFOS, R. 1995 Decay of dipolar vortex structures in a stratified fluid. *Phys. Fluids* **7**, 374–383.
- VAN GEFFEN, J. H. G. M. & VAN HEIJST, G. J. F. 1998 Viscous evolution of 2D dipolar vortices. *J. Geophys. Res.* **22**, 191–213.
- GODEFERD, F. S. & STAQUET, C. 2003 Statistical modelling and direct numerical simulations of decaying stably stratified turbulence. Part 2. Large-scale and small-scale anisotropy. *J. Fluid Mech.* **486**, 115–159.
- GODOY-DIANA, R., CHOMAZ, J. & BILLANT, P. 2003 Vertical length scale selection for pancake vortices in strongly stratified viscous fluids. *J. Fluid Mech.* **504**, 229–238.
- GOURLAY, M. J., ARENDT, S. C., FRITTS, D. C. & WERNE, J. 2001 Numerical modeling of initially turbulent wakes with net momentum. *Phys. Fluids* **13**, 3783–3802.
- HOPFINGER, E. J., BROWAND, F. K. & GAGNE, Y. 1982 Turbulence and waves in a rotating fluid. *J. Fluid Mech.* **125**, 505–534.
- HULD, T., NIELSEN, A. H., PCSELI, H. L. & RASMUSSEN, J. J. 1991 Coherent structures in two-dimensional plasma turbulence. *Phys. Fluids B* **3**, 1609–1625.

- LAMB, H. 1932 *Hydrodynamics*. Cambridge University Press.
- LILLY, D. K. 1983 Stratified turbulence and the meso-scale variability of the atmosphere. *J. Atmos. Sci.* **40**, 749–761.
- LIN, J. T. & PAO, Y. H. 1979 Wakes in stratified fluids. *Annu. Rev. Fluid Mech.* **11**, 317–338.
- LISKA, R. & WENDROFF, B. 1998 Composite schemes for conservation laws. *SIAM J. Numer. Anal.* **35**, 2250–2271.
- MELESHKO, V. V. & VAN HEIJST, G. J. F. 1994 On Chaplygin’s investigations of two-dimensional vortex structures in an inviscid fluid. *J. Fluid Mech.* **272**, 157–182.
- NGUYEN DUC, J. M. & SOMMERIA, J. 1988 Experimental characterization of steady two dimensional vortex couples. *J. Fluid Mech.* **192**, 175–192.
- NIELSEN, A. H. & RASMUSSEN, J. J. 1997 Formation and temporal evolution of the Lamb-dipole. *Phys. Fluids* **9**, 982–991.
- PRAUD, O. & FINCHAM, A. M. 2000 3D dipolar vortex structures in stably stratified fluids. *Proc. Fifth Intl Symp. on Stratified Flows, Vancouver, Canada*, vol. 1, pp. 107–112.
- PRAUD, O., FINCHAM, A. M. & SOMMERIA, J. 2005 Decaying grid turbulence in a strongly stratified fluid. *J. Fluid Mech.* **522**, 1–33.
- RILEY, J. J. & LELONG, M. P. 2000 Fluid motion in the presence of strong stable stratification. *Annu. Rev. Fluid Mech.* **32**, 613–657.
- RILEY, J. J., METCALFE, R. W. & WEISSMAN, M. A. 1981 Direct numerical simulation of homogeneous turbulence in density-stratified fluids. *Proc. Conf. on Nonlinear Properties of Internal Waves* (ed. J. B. West) pp. 79–112.
- SOUS, D., BONNETON, N. & SOMMERIA, J. 2004 Turbulent vortex dipoles in a shallow water layer. *Phys. Fluids* **16**, 2886–2898.
- SPEEDING, G. R. 2002 Vertical structure in stratified wakes with high initial froude number. *J. Fluid Mech.* **454**, 71–112.
- SPEEDING, G. R., BROWAND, F. K. & FINCHAM, A. M. 1996 Turbulence, similarity scaling and vortex geometry in the wake of a sphere in a stably stratified fluid. *J. Fluid Mech.* **314**, 53–103.
- SWATERS, G. E. 1988 Viscous modulation of the Lamb dipole vortex. *Phys. Fluids* **31**, 2745–2747.
- TURNER, J. S. 1964 The flow into an expanding spherical vortex. *J. Fluid Mech.* **18**, 195–208.
- VOROPAYEV, S. I., AFANASYEV, Y. D. & FILIPPOV, I. A. 1991 Horizontal jets and vortex dipoles in a stratified fluid. *J. Fluid Mech.* **227**, 543–566.
- VOROPAYEV, S. I., AFANASYEV, Y. D. & VAN HEIJST, G. J. F. 1995 Two-dimensional flows with zero net momentum: evolution of vortex quadripoles and oscillating grid turbulence. *J. Fluid Mech.* **282**, 21–44.
- VOROPAYEV, S. I., SMIRNOV, S. A. & BRANDT, A. 2001 Dipolar eddies in a stratified shear flow. *Phys. Fluids* **13**, 3820–3823.